数理解析研究所講究録
第1970巻 2015年 90-95

Density of states and conductance in disordered topological insulator surfaces

Tomi OHTSUKI*, Koji KOBAYASHI† and Vincent SACKSTEDER‡

April 30, 2015

Abstract

Disorder induced metal-insulator transition, the Anderson transition, usually occurs in the region where the density of states is smooth and shows no singularity. In the semimetal to metal transition, however, the density of states is critical. This phenomenon is attracting new interests in relation to the topological insulator where Dirac and Weyl semimetals undergo semimetal to metal transition. In this paper, we review the recent progress of the scaling behavior of the density of states and conductance at this semimetal to metal transition.

1 Introduction

Disorder induced metal-insulator transition, the Anderson transition, is characterized by the vanishing conductivity $\sigma(x)$ and the diverging length scale ξ,

$$\sigma \sim (x - x_c)^{s_A}\,,\ \xi \sim \frac{1}{|x - x_c|^{\nu_A}}\,,\ s_A = (d-2)\nu_A \tag{1}$$

where x is a parameter such as strength of disorder W, Fermi energy ϵ, and pressure. d is the dimensionality and the last equation is called Wegner's relation[1]. Here we have assumed that $x > x_c$ is the metal phase. At the Anderson transition, the density of states $\rho(\epsilon)$ is smooth and shows no singularity at the transition.

In the case of semimetal where the Fermi energy is located at Dirac/Weyl node, or at the band edge, the density of states at energy $\epsilon = 0$ is vanishing. As we change the parameter,*e.g.*, as we increase the disorder, the vanishing density of states becomes finite at finite disorder W_c [2],

$$\rho(0) \sim (W - W_c)^{\beta}\,, \tag{2}$$

which is called semimetal to metal transition. Here we have neglected the exponentially small tails, which becomes important for the case of long ranged randomness [3].

In the standard parabolic dispersion $\epsilon = \hbar^2 k^2/2m$, however, this is difficult to observe. To show this intuitively, we follow the argument by Syzranov *et al.* [4]. For long wave length, the impurity potentials are averaged over the wave length λ, and the effective impurity strength $W_{\rm eff}$ for the wave function with the wave number k is estimated to be

$$W_{\rm eff}(k) \sim \frac{W}{\sqrt{\lambda^d}} \sim \sqrt{k^d}\,. \tag{3}$$

*Department of Physics, Sophia University, Kioi-cho 7-1, Chiyoda-ku, Tokyo 102-8554, Japan.
e-mail: ohtsuki@sophia.ac.jp
†Department of Physics, Sophia University, Kioi-cho 7-1, Chiyoda-ku, Tokyo 102-8554, Japan.
e-mail: k-koji@sophia.ac.jp
‡School of Physical and Mathematical Sciences, Nanyang Technological University, 637371, Singapore
e-mail: vincent@sacksteder.com

Assuming the dispersion $\epsilon(k) = A|k|^a$ where the density of states is

$$\rho(\epsilon) \sim \epsilon^{d/a-1}, \tag{4}$$

we compare the potential energy W_{eff} with the kinetic energy $\epsilon(k)$, and obtain

$$\frac{W_{\text{eff}}(k)}{\epsilon(k)} \sim k^{(d-2a)/2}. \tag{5}$$

This means for $d > 2a$, the effect of randomness vanishes for low energy (large wave length), and randomness is irrelevant up to certain strength of disorder, i.e., W_c [5]. Since most of the three dimensional (3D) material shows parabolic dispersion $a = 2$, the disorder induced semimetal to metal transition can not be observed; the density of states becomes finite once W is finite. Recent discovery of 3D material with linear dispersion (Dirac electron) in topological insulators makes this situation experimentally possible. In this case, $d = 3$ and $a = 1$, and the disorder is irrelevant for small W.

2 Model for 3D Dirac system

The 3D Dirac electrons emerge in Wilson-Dirac Hamiltonian,

$$\begin{aligned} H = & \sum_{\vec{r}} \sum_{\mu=x,y,z} \left[|\vec{r} + \vec{e}_\mu\rangle \left(\tfrac{it}{2}\gamma_\mu - \tfrac{m_2}{2}\gamma_0 \right) \langle \vec{r}| + \text{h.c.} \right] \\ & + \sum_{\vec{r}} |\vec{r}\rangle \Big[(m_0 + 3m_2)\gamma_0 + V_{\vec{r}} 1_4 \Big] \langle \vec{r}|, \end{aligned} \tag{6}$$

where $\vec{e}_\mu$ is a unit vector in the μ-direction, and 1_4 represents the 4×4 identity matrix. γ_μ and γ_0 form a set of γ-matrices in a 4×4 representation,

$$\gamma_\mu = \begin{pmatrix} 0 & \sigma_\mu \\ \sigma_\mu & 0 \end{pmatrix}, \ \gamma_0 = \begin{pmatrix} 1_2 & 0 \\ 0 & -1_2 \end{pmatrix}, \tag{7}$$

where σ_μ's are Pauli matrices and 1_2 is 2×2 identity matrix. m_0, m_2 and t are mass and hopping parameters. For $W = 0$, the energy is expressed by

$$\epsilon(k) = \pm\sqrt{[m_0 + m_2(3 - (\cos k_x + \cos k_y + \cos k_z))]^2 + t^2(\sin^2 k_x + \sin^2 k_y + \sin^2 k_z)}, \tag{8}$$

and the gap closes at $m_0/m_2 = 0, -2$ for $\vec{k} = (0,0,0)$ and $\vec{k} = (\pi,0,0), (0,\pi,0), (0,0,\pi)$. For $-2 < m_0/m_2 < 0$ the system is in the strong topological insulator phase, while for $-4 < m_0/m_2 < -2$ the system is in the weak topological insulator phase. ($m_0/m_2 > 0$ corresponds to the ordinary insulator.) $V_{\vec{r}}$ represents a potential disorder distributed uniformly and independently between $-W/2$ and $W/2$.

By tuning the gap parameter m_0/m_2, the band gap closes, and the Dirac/Weyl nodes appear with $\epsilon = \hbar v k$, $v = t$. At this point, the low energy density of states is

$$\rho(\epsilon) \sim \epsilon^2/v^3,$$

In the presence of disorder, similar parabolic dependence on energy is seen with m_0 and v renormalized. It should be noted that the ordinary insulator region is invaded by the topological insulator phase, which is contrary to the intuition that disorder destroys order. This enhancement of the topological phase due to disorder is dubbed topological Anderson insulator, and has been discovered theoretically in 2D [6, 7, 8, 9], and in 3D [10, 11].

3 Scaling behavior

To describe the scaling behavior, we follow the discussion by Kobayashi *et al.* [12], and begin with a dimensionless quantity, the number of states $N(\epsilon, L)$ below the energy ϵ in the cubic system of size L, and assume that it is a function of dimensionless parameters L/ξ and ϵ/ϵ_0,

$$N(\epsilon, L) = F(L/\xi, \epsilon/\epsilon_0)\,, \tag{9}$$

where ξ and ϵ_0 are the characteristic length and energy scales, respectively. They are related by the dynamical exponent z,

$$\epsilon_0 \propto \xi^{-z}\,. \tag{10}$$

Since $N(\epsilon, L)$ is proportional to L^d for large L, the above scaling form should be

$$N(\epsilon, L) = (L/\xi)^d f(\epsilon\xi^z)\,. \tag{11}$$

From $N(\epsilon, L)$, the DOS per volume $\rho(\epsilon)$ is calculated as

$$\rho(\epsilon) = \frac{1}{L^d}\frac{dN(\epsilon, L)}{d\epsilon}\,, \tag{12}$$

and we obtain its scaling form,

$$\rho(\epsilon) = \rho(-\epsilon) = \xi^{z-d} f'(|\epsilon|\xi^z)\,. \tag{13}$$

We introduce the distance from the critical point $\delta = |W - W_c|/W_c$, and assume that ξ diverges near the critical point W_c as,

$$\xi \sim \delta^{-\nu}\,, \tag{14}$$

where ν is the critical exponent. Close to the critical point, we thus obtain from Eq. (13)

$$\rho(\epsilon) \sim \delta^{(d-z)\nu} f'(|\epsilon|\delta^{-z\nu})\,. \tag{15}$$

Let us examine the consequence of this scaling form in the semimetal and metal phases.

3.1 Semimetal phase

If the system has Dirac node, the DOS is expected to be proportional to $|\epsilon|^{d-1}$ for $|\epsilon| \ll \epsilon_0$, so

$$\rho(\epsilon) \sim \delta^{(d-z)\nu}(|\epsilon|\delta^{-z\nu})^{d-1} = |\epsilon|^{d-1}\delta^{-(z-1)d\nu}\,. \tag{16}$$

Since the prefactor $\delta^{-(z-1)d\nu}$ should be proportional to $1/v(W)^d$, the renormalization of the velocity should read

$$v(W) \sim \delta^{(z-1)\nu}\,. \tag{17}$$

3.2 Metal phase

On the other hand, $\rho(\epsilon)$ is finite at $\epsilon = 0$ in the metal phase, and

$$\rho(0) \sim \delta^{(d-z)\nu}(|\epsilon|\delta^{-z\nu})^0 = \delta^{(d-z)\nu}\,, \tag{18}$$

and from Eq. (2), we obtain

$$\beta = (d - z)\nu\,. \tag{19}$$

3.3 Critical point

Right at the critical point $\delta = 0$, ξ dependencies should cancel, and

$$\rho(\epsilon) \sim \delta^{(d-z)\nu}(|\epsilon|\delta^{-z\nu})^{(d-z)/z} = |\epsilon|^{(d-z)/z}\,. \tag{20}$$

3.4 Diffusion and conductivity

The general scaling arguments imply interesting transport properties as well. Consider, for example, the wave packet dynamics [13]. We assume the mean square displacement $\langle \vec{r}^2(t,\epsilon)\rangle$ of the state with energy ϵ at time t, where $\langle\cdots\rangle$ represents both quantal and ensemble averages to be of the form

$$\langle \vec{r}^2(t,\epsilon)\rangle \sim \xi^2 g(t\xi^{-z}, |\epsilon|\xi^z)\,. \tag{21}$$

In the metal phase, one expects $\langle \vec{r}^2(t,\epsilon)\rangle = 2dD(\epsilon)t$ for large t with $D(\epsilon)$ the diffusion coefficient at energy ϵ. We focus only on the state with $\epsilon = 0$ and obtain the scaling form,

$$\langle r^2(t,\epsilon=0)\rangle \sim \xi^{2-z}t\,, \tag{22}$$

and the diffusion constant $D(\epsilon=0)$ scales with

$$D(\epsilon=0) \sim \xi^{2-z} \sim \delta^{-(2-z)\nu}\,, \tag{23}$$

which diverges towards the critical point (as will be discussed in Section 5, the estimate of z for 3D Dirac/Weyl systems is 1.5, well below 2). Combined with the density of states, the conductivity σ is obtained as

$$\sigma(\epsilon=0) \sim \rho(\epsilon=0)D(\epsilon=0) \sim \delta^{(d-2)\nu}\,, \tag{24}$$

and the Wegner's relation is recovered. Note, however, that $\nu \neq \nu_A$ (see Eq. (1)).

4 Density of state scaling in other systems

The novel scaling of the density of states is now predicted in several different systems, and we now turn our attention to the cases of 2D, $d > 4$ and $d = 1$.

4.1 2D case (surface disorder)

When we have a bulk gap, the topological insulator shows surface states with linear dispersion, *e.g.*, $\epsilon = \hbar v\sqrt{k_x^2 + k_y^2}$ on the surface perpendicular to z-direction. When the surface is disordered while bulk of the system is clean, we observe the surface states are robust against disorder, and the density of states remains to be linear in ϵ, while the slope gets steeper, which means again the renormalization of the velocity. Velocity renormalization is also seen for 2D topological insulator with edge disorder [14].

Once the strength of disorder exceeds critical value, $\rho(0)$ becomes finite. This behavior is similar to what we have observed for the 3D Dirac semimetal.

We demonstrate this behavior by using the above Wilson-Dirac Hamiltonian, Eq. (6), and by assuming that the randomness exists only at the surfaces [15]. In Figure 1, we show the density of states for a rectangular parallelepiped of size $400\times400\times20$ (in units of lattice constant). Periodic boundary conditions are imposed in x- and y-directions, while open boundary condition is imposed in z-direction. The gap parameter m_0/m_2 is -1, so the bulk is a strong topological insulator. Randomness exists only at the top and the bottom layers. Kernel polynomial method is used for the actual numerical calculation [16].

4.2 High and low dimensional cases of orthogonal universality class

The scaling of the density of states has been generalized in ref.[4] for high dimensional systems belonging to the Wigner-Dyson orthogonal class [17, 18, 19]. The one dimensional case with small a ($\epsilon \sim |k|^a$, $a < 1/2$) is also discussed in [20]. They all show similar scaling behavior of the density of states. (See figure 2 of ref.[12], figure 1 of this article, and figure 1 of ref.[20].)

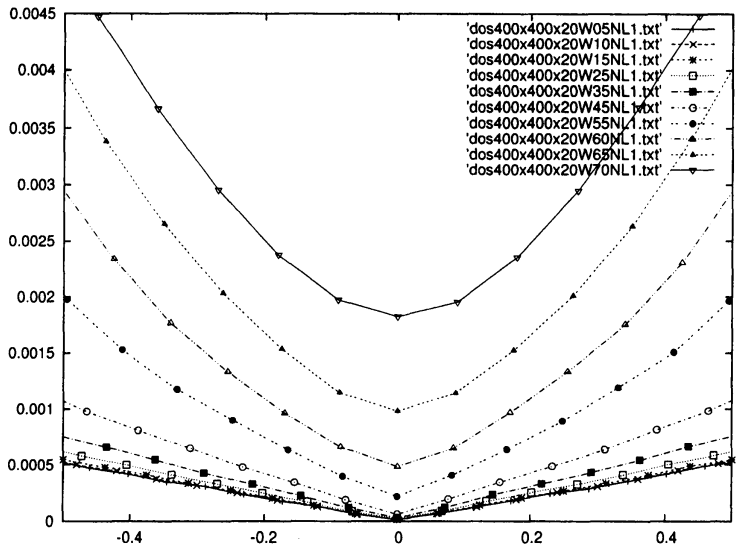

Figure 1: Density of states for surface states in the 3D topological insulator with surface disorder. The system is a rectangular parallelepiped of size $400 \times 400 \times 20$. The strength of surface disorder W is varied from 0.05 to 0.7. At small disorder $W \leq 4.5$ the dispersion is linear in ε , which means the surface Dirac electron states are robust against disorder. The increase of the slope corresponds to the renormalization of the velocity with W. Once W exceeds critical value $4.5 < W_c < 5.5$, the zero energy density of states becomes finite.

5 Estimate of exponents

By calculating the density of states for the cubic system of size $200 \times 200 \times 200$, ν and z for 3D Dirac/Weyl systems are estimated as $\nu = 0.9 \pm 0.2$ and $z = 1.5 \pm 0.1$ [12]. These values are to be compared with the values for 3D Anderson transition of symplectic universality class, $\nu_A = 1.375 \pm 0.08$ and $z_A = 3$ [21, 22], which are significantly different from the cases of semimetal to metal transition.

The single parameter scaling , Eq. (15), predicts that when we plot $\rho(\epsilon)/\delta^{(d-z)\nu}$ against $|\epsilon|\delta^{-z\nu}$, all the plots of the density of states with various W are on two branches, i.e., the semimetal branch and the metal branch. This has also been verified numerically.

Analytic estimate of ν and z by one-loop renormalization group analysis is successful for the 3D Dirac/Weyl fermions (Wigner-Dyson symplectic universality class [17, 18, 19]). In ref. [10], ν and z are estimated to be 1 and 3/2, respectively, which are in excellent agreement with the above numerical estimate. The self-consistent Born approximation (SCBA) gives the estimate $\beta = 1$[23]. Combined with $z \approx 1.5$ and Eq. (18), the estimate $\nu \approx 2/3$, which is close to the lower bound of ν, $2/d = 2/3$[24]. From SCBA, we can also estimate the conductivity exponent $s = 1$, which is close to the numerical estimate $s = (d-2)\nu = 0.9 \pm 0.2$.

In the case of orthogonal universality class, we can estimate $\nu = 1/(d-2a)$ and $z = 1 + (d-2a)/4$ by one-loop renormalization group analysis [4]. This should be check by numerics in the future.

6 Summary

In summary, the semimetal to metal transition at the Dirac/Weyl nodes and at band edge are well described by the scaling of the density of states, which is supported by the numerical evidence. From the metal side, the density of states vanishes while the diffusion constant diverges as we decrease the disorder. The conductivity, however, still behaves the same way as in the Anderson transition, and the

Wegner's relation holds. Further numerical as well as analytical studies are needed to clarify this novel phase transition quantitatively.

References

[1] F. Wegner, Z. Phys. B **25**, 327 (1976).

[2] E. Fradkin, Phys. Rev. B **33**, 3263 (1986).

[3] R. Nandkishore, D.A. Huse, and S. L. Sondhi, Phys. Rev. B **89**, 245110 (2014)

[4] S.V. Syzranov, V. Gurarie, L. Radzihovsky, Phys. Rev. B **91**, 035133 (2015).

[5] R. Shindou, S. Murakami, Phys. Rev. B **79**, 045321 (2009).

[6] J. Li, R.-L. Chu, J.K. Jain, S.-Q. Shen, Phys. Rev. Lett. **102**, 136806 (2009).

[7] C. W. Groth, M. Wimmer, A. R. Akhmerov, J. Tworzydo, C. W. J. Beenakker, Phys. Rev. Lett. **103**, 196805 (2009).

[8] H.-M. Guo, G. Rosenberg, G. Refael, M. Franz, Phys. Rev. Lett. **105**, 216601 (2010).

[9] D. Xu, J. Qi, J. Liu, V. Sacksteder, X.-C. Xie, H. Jiang, Phys. Rev. B, **85**, 195140 (2012).

[10] P. Goswami, S. Chakravarty, Phys. Rev. Lett. **107**, 196803 (2011).

[11] K. Kobayashi, T. Ohtsuki, K.-I. Imura, Phys. Rev. Lett. **110**, 236803 (2013).

[12] K. Kobayashi, T. Ohtsuki, K.-I. Imura, I. Herbut, Phys. Rev. Lett. **112**, 016402 (2014).

[13] T. Ohtsuki, T. Kawarabayashi, J. Phys. Soc. Jpn. **66**, 314 (1997).

[14] Q.Wu, L. Du, V. Sacksteder, Phys. Rev. B **88**, 045429 (2013).

[15] V. Sacksteder, T. Ohtsuki, K. Kobayashi, arXiv:1410.7621.

[16] A. Weisse, G. Wellein, A. Alvermann, H. Fehske, Rev. Mod. Phys. **78**, 275 (2006).

[17] E.P. Wigner, Proc. Cambridge Philos. Soc. **47**,790 (1951).

[18] F.J. Dyson, J. Math. Phys. **3**, (1962) 140; **3** (1962) 157; **3** (1962) 166.

[19] M.L. Mehta, *Random matrices*, Academic Press, Boston (1991).

[20] M. Garttner, S.V. Syzranov, A.M. Rey, V. Gurarie, L. Radzihovsky, arXiv:1504.05971.

[21] Y. Asada, K. Slevin, T. Ohtsuk, J. Phys. Soc. Jpn. Suppl. **74**, 238 (2005).

[22] K. Slevin, T. Ohtsuki, New J. Phys. **16**, 015012 (2014).

[23] Y. Ominato, M. Koshino, Phys. Rev. B **89**, 054202 (2014).

[24] J.T. Chayes, L. Chayes, D.S. Fisher, T. Spencer, Phys. Rev. Lett. **57**, 2999 (1986).